Nanostructured TiO_2/carbon nanosheet hybrid electrode for high-rate thin-film lithium-ion batteries

S. Moitzheim[1,2,4], C. S. Nimisha[1,2,4], Shaoren Deng[3,4], Daire J. Cott[1], C. Detavernier[3], P. M. Vereecken[1,2]

[1]Imec, Kapeldreef 75, B-3001 Leuven, Belgium

[2]Centre of Surface Chemistry and Catalysis, University of Leuven, B-3001, Leuven, Belgium

[3]Department of Solid State Science, Ghent University, Krijgslaan 281/S1, B-9000 Ghent, Belgium.

[4]Contributed equally

Abstract

Heterogeneous nanostructured electrodes using carbon nanosheets (CNS) and TiO_2 exhibit high electronic and ionic conductivity. In order to realize chip level power sources, it is necessary to employ microelectronic compatible techniques for fabrication and characterization of TiO_2-CNS thin-film electrodes. To achieve this, vertically standing CNS grown through a catalytic free approach on a $TiN/SiO_2/Si$ substrate by plasma enhanced chemical vapour deposition (PECVD) was used. The substrate attached CNS is responsible for sufficient electronic conduction and increased surface-to-volume ratio due to its unique morphology. Atomic layer deposition (ALD) of nanostructured amorphous TiO_2 on CNS provide enhanced Li storage capacity, high rate performance and stable cycling. The amount of TiO_2 deposited masks the underlying CNS, thereby controlling the accessibility of CNS which gets reflected in the total electrochemical performance as revealed by cyclic voltammetry and charge/discharge measurements. TiO_2 thin-films deposited with 300, 400 and 500 ALD cycles on CNS have been studied to understand the kinetics of Li insertion/extraction. A large potential window of operation (3 - 0.01 V), excellent cyclic stability with a capacity retention of 98% of the initial value and remarkable rate capability up to 100C, are the highlights of TiO_2/CNS thin film anode structures. CNS with an optimum amount of TiO_2 coating is proposed as a promising approach for the fabrication of electrodes for chip compatible thin-film Li-ion batteries.

Keyword: Heterogeneous electrode, Carbon nanosheets, Atomic layer deposition, High rate capability

1. Introduction

1.1 Carbon nanosheets

Heterogeneous electrodes are tailored to address diverse requirements when used as anode or cathode for Li-ion batteries (LIB). Improved electronic and ionic conduction, stable cycling behaviour, and ease of integration with the electrolyte are some of the qualities contributed by the individual components of a heterogeneous electrode structure. Nanostructuring the components involved is a straightforward approach to enhance the electrochemical performance of bulk materials which benefits from a shortening of the Li-ion insertion/extraction pathway and enhanced lithium storage capabilities due to changes in solubility limits of the host material [1].

For this reason, carbon nanosheets (CNS, or alternatively called graphene nanosheets) that have a high surface-to-volume ratio due to their petal like arrangement, attracted much attention as a potential anode for LIB [2], [3]. The capacity of CNS (740-780 mAh/g) was found to be double than that of bulk graphite, which is the current anode material in commercially available LIBs. This enhanced capacity was shown to be related to the increased distance between the carbon sheet spacing which changes the electronic properties and facilitates Li^+ insertion/extraction [2]. Carbon nanosheets can furthermore be fabricated free-standing and vertically oriented on a (conductive) substrate (so-called substrate-attached CNS), giving rise to a three dimensional interconnected network of highly conducting sheets. [4] Only a few studies on such substrate-attached CNS and their lithium insertion/extraction properties have been reported so far [5], [6]. Kim et al. reported highly branched CNS grown on a copper substrate by plasma enhanced chemical vapor deposition (PECVD); a specific capacity of 500 mAh/g at a current density of 50 mA/g was achieved with 10% irreversible capacity loss after 100 cycles. This electrode could furthermore deliver a stable capacity of 300 mAh/g at a rate of 1000 mA/g [5]. Xiao et al. reported on the performance of CNS grown on a Ni substrate by PECVD [6]. Nickel was used as catalyst during fabrication and as current collector during electrochemical characterization. This type of substrate-attached CNS electrode also resulted in a reversible capacity of 280 mAh/g at 1000 mA/g, similar to the one of Kim et al. [5]. However, after being charged/discharged for 150 cycles at different rates, the capacity dropped to ~82% of the original reversible capacity. Furthermore, even though CNS have a very high gravimetric capacity due to its mesoporous nature, the volumetric capacity is

however limited. This can be remedied by filling the open space with another active material and combining both the high electric conductivity as well as the short diffusion path due to the nanostructure morphology.

1.2 TiO2/carbon nanosheet hybrid

In order to improve the stability and volumetric capacity of the electrode, CNS can be coated with another active electrode material that shows good stability. A material that has been widely studied as an active electrode material of LIB due to its structural characteristics, special surface activity, abundance, low cost, and environmental benignity, is TiO_2 [7], [8]. Titanium dioxide is capable of intercalating Li^+ ions with reduction of the Ti(IV) transition metal to Ti(III) [15]. The formula for this chemical reaction can be written as

$$x\mathrm{Li}^+ + x\mathrm{e}^- + \mathrm{TiO_2} \leftrightarrow \mathrm{Li}x\mathrm{TiO_2}\ (0 \le x \le 1), \qquad (1)$$

which leads to a theoretical capacity of ~330 mAh/g for $x = 1$ when TiO_2 has the anatase crystal structure. However, the poor electronic conductivity (~ 10^{-8} - 10^{-12} S/m, [9]) and low Li^+ diffusion in TiO_2 (10^{-10} cm^2/s – 10^{-17} cm^2/s, [10]) are detrimental for the rate performance of lithium insertion/extraction. These shortcomings can, however, be remedied by combining the fast electron transport of CNS [11] and the nanosizing of TiO_2 to decrease the Li^+ diffusion length. Different reports have already shown the benefits of combining TiO_2 with CNS to form high-power electrodes as the anode of LIB [12]–[14]. However, these reports made use of CNS synthesized by reduction of graphite oxide and subsequent solvent based TiO_2 deposition, and not substrate attached CNS that offers excellent contact to the underlying current collector.

Recently, an electrode fabricated by depositing amorphous TiO_2 using ALD on CNS (synthesized by reduction of graphene oxide) was shown to deliver a stable capacity of 100 mAh/g at a current density of 2000 mA/g (~6 C) with 95% of the original capacity after 500 cycles [15]. Because of the difficulty of nucleating the TiO_2 ALD films on sp^2 carbon planes, an Al_2O_3 ALD adhesion layer was necessary. Although, reasonably high-power density could be achieved, this Al_2O_3 layer likely increased the resistance for the electrons which in turn limits the performance. Furthermore this approach severely diminishes the superior qualities of CNS, since intra-sheet electron conduction and contact with the current collector will be hindered by the Al_2O_3/TiO_2 interface. Additionally, the electrode was

fabricated by mixing slurry of the composite with which is not useable for integration with conventional CMOS fabrication techniques.

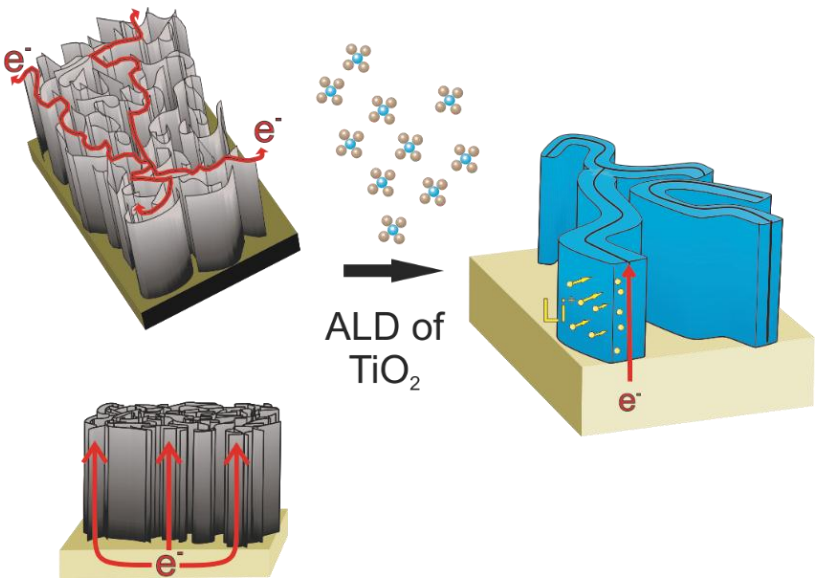

Figure 1. Schematic of electron conduction in carbon nanosheets, and their use as a 3D substrate for TiO_2. The fast electron transport and short Li+ diffusion path leads to a high power density.

1.3 Substrate attached TiO_2-CNS

We have previously shown that CNS grown with (PECVD) can produce vertically standing CNS on a large area TiN/SiO_2/Si substrate [4]. The robust electrical contact to the underlying TiN lead to a low resistivity of ~20 μΩ cm. This is very interesting from the point of view of using CNS as 3D current collector and/or as the anode for thin-film LIB. Furthermore, the CNS are grown with defects which give rise to nucleation sites for ALD TiO_2, allowing for conformal deposition [16]. Even after coating of the surface with TiO_2, the interconnected nature of the CNS and good contact to the current collector are maintained, which allows electrons to easily flow throughout the CNS structure as illustrated in figure 1, while keeping the Li^+ diffusion distance short.

In this work we studied the balance between performance and capacity as a function of a different thickness (15 – 25 nm) of ALD deposited amorphous TiO_2 on substrate attached CNS. Remarkable rate capability and stable cyclic performance is achieved. It is shown that the film thickness of TiO_2 has an effect on the kinetics of Li^+ storage mechanism. Furthermore, the fabrication steps involved in this work are compatible with existing micro fabrication and processing techniques for integrated micro systems.

2. Experimental details

2.1 Preparation of vertically standing CNS on TiN/Si substrate.

A 200 mm silicon wafer with 90 nm thermal SiO_2 coated with 70nm TiN was used as the carrier for deposition. The TiN layer was deposited by sputtering from a Ti target in a N_2 atmosphere (Applied Endura Extensa TTN). The TiN layer served as the electrical contact to the CNS and lithium diffusion barrier for the underlying Si. CNS films were grown in a PECVD chamber capacitively coupled with an RF (13.56MHz) source (Oxford Instruments Plasma Technology UK). In brief, the growth of the CNS was initiated by heating the TiN covered wafer to 750° C under vacuum (10^{-6} mbar) for 1 minute. A H_2 plasma pre-treatment (300W) was carried out for 15 minutes at 0.6 mbar. C_2H_2 was added to the H_2 plasma at a 1:10 ratio (C_2H_2:H_2) for 45 minutes. The CNS covered wafer was removed from the chamber and allowed to cool under vacuum (10^{-4} mbar) for 5 minutes.

2.2 ALD of TiO_2 on CNS.

Different samples were cleaved from the CNS covered wafer in 2x2 cm pieces and were loaded into a home-built ALD reactor with base pressure of $5x10^{-7}$ mbar. Before starting the ALD cycles, the sample was heated to 100 ºC and kept at this temperature for 1h. One ALD cycle of TiO_2 consisted of applying alternately for 20 s each a pulse of tetrakis(dimethylamido)titanium (TDMAT) (99.999% Sigma-Aldrich) at $3x10^{-1}$ mbar and a pulse of ~150 µg/ mL ozone (produced by ozone generator, Yanco Industries, LTD) at $5x10^{-1}$ mbar. To completely remove all the residual gases between each precursor pulse, the reactor was evacuated for 40 s to a pressure of $1\sim2x10^{-5}$ mbar. By varying the amount of cycles (*i.e.* 300, 400 and 500 cycles), different thicknesses of TiO_2 were deposited on the CNS. To determine the influence of the CNS and TiO_2 separately, TiO_2 was also grown using the same amount of cycles without CNS on the TiN substrate.

2.3 Structural characterization

X-ray diffraction (XRD) was performed on a BrukerD8 system diffractometer, equipped with Cu Kα radiation by scanning in the 2ϑ range in grazing incidence mode. The TiO_2/CNS films were analyzed by scanning electron microscopy (SEM) and Raman spectroscopy (Jobin-Yvon spectrometer, 0.3 cm^{-1} spectral resolution, laser power

of 0.5 mW). The equivalent thickness of TiO_2 after 300, 400 and 500 ALD cycles was determined by X-ray fluorescence (XRF) measurement (Bruker, ARTAX system) of the Ti content.

2.3 Electrochemical testing of TiO_2/CNS electrodes

Electrochemical measurements were performed using a custom built three-electrode glass cell. The glass cell was clamped onto 2 cm x 2 cm samples using a Viton O-ring. The geometrical surface area of the exposed electrode was 1.43 cm^2. Lithium metal sheet and wire were used as counter and reference electrode, respectively. The Li reference electrode was placed in a glass capillary with the tip placed less than 1 mm from the electrode surface. Contact was made to the bare TiN underlayer with a crocodile clip at the edge of the sample (outside glass cell). The electrolyte used was 1.0 M $LiPF_6$ in a 50:50 (v/v) mixture of ethylene carbonate (EC) and diethyl carbonate (DEC) (LP40, Merck). All the operations on the cell assembly were carried out in a glove box (InertLab) filled with argon gas where both water and oxygen concentrations were less than 1 ppm. A potentiostat/galvanostat Autolab PGSTAT30 (Metrohm Autolab) was used to perform all of the electrochemical experiments, which was controlled through the Nova 1.8 software. All voltages are given *vs* Li^+/Li.

Cyclic voltammograms (CV) were recorded starting from open-circuit potential between 3.00 V and 0.01V at different scan rates (0.5 - 500 mV/s). Subsequently, galvanostatic cycling was performed between 3.00 V - 0.01 V at various current densities (C-rates) to evaluate the rate and cycle performance. For the charging rate, 1C was determined based on the charge calculated from the discharge capacity with a 0.5 mV/s CV.

3. Results and Discussion

3.1 Structure and morphology of the as-prepared and TiO_2-coated CNS

The SEM images of as-prepared and ALD TiO_2 coated CNS on the $TiN/SiO_2/Si$ substrate is shown in figure 2. The top-down SEM image (figure 2a) shows the corrugated petal-like arrangement of as-prepared CNS that leads to its high surface-to-volume ratio. A Raman spectrum of as-prepared CNS is shown in figure S1 and exhibits well distinguished D and G peaks together with second-order peaks. A peak intensity ratio I_D/I_G [17] of 2.6 indicates the sheets are defective with an average crystallite size (*La*) of 2.68 nm, indicating at the very least there are sites available every 2.68 nm along the edge and basal surface of a 700 nm sheet where nucleation of ALD deposited TiO_2 can take place. Detailed description of Raman spectral behaviour of surface attached CNS can be found in ref. [4].

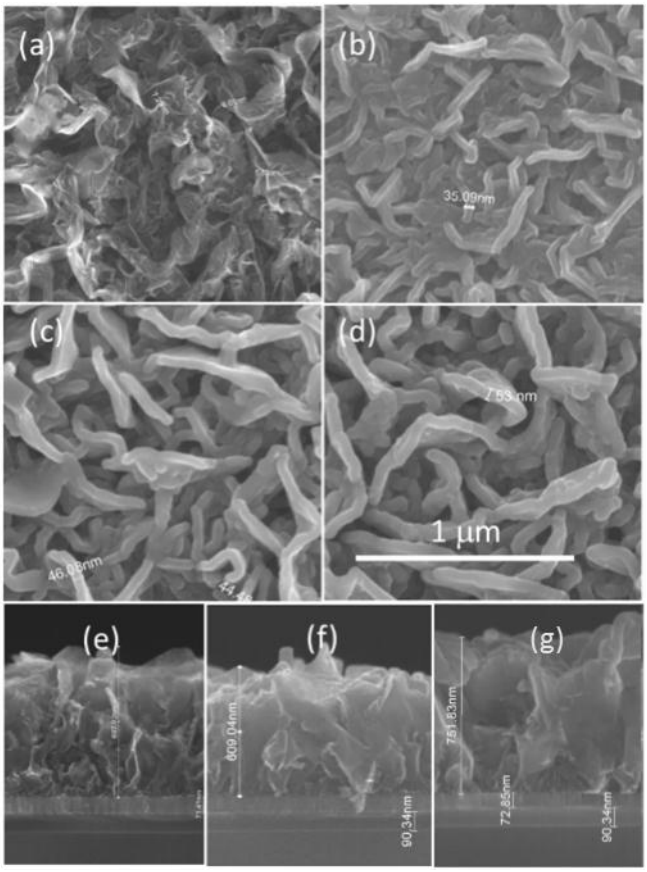

Figure 2. SEM images of bare CNS and TiO_2-CNS; (a) top view of bare CNS; (b) top view of 15 nm TiO_2-CNS, (c) 20 nm TiO_2-CNS and (d) 25 nm TiO_2 on CNS; (e-g) side view of 15, 20 and 25 nm TiO_2-CNS.

After TiO_2 deposition, the resulting surface morphology can be seen in the top view SEM image of figure 2b-d. By varying the number of ALD cycles between 300 (figure 2b), 400 (figure 2c) and 500 (figure 2d) cycles, a different thickness of TiO_2 on the CNS composite was obtained. Figure 2e-g also shows the cross-section SEM image for 300, 400 and 500 ALD TiO_2 on CNS, showing a height of ~600-750 µm and the coverage of TiO_2 inside the CNS structure. The top-view SEM images of figure 2b-d give a rough estimate of the thickness of the TiO_2/CNS/TiO_2 sheets. For 300 cycles ALD, the thickness is ~35 nm, which increases for 400 and 500 cycles ALD to ~50 and ~60 nm respectively. This is roughly in accordance with the nominal thickness of TiO_2 based on the ALD growth rate of 0.05 nm/cycle for a CNS thickness of 10 nm and taking into account that the TiO_2 can deposit on both sides of the exposed CNS (see table 1). The equivalent thicknesses of deposited TiO_2 for different ALD cycles based on the Ti content has also been obtained from XRF measurements and are given in table 1.

Table 1. Thickness of TiO_2 determined with different techniques with the corresponding area enhancement and theoretical capacity.

# of ALD cycles	Equivalent thickness TiO_2 from XRF signal (nm)	Theoretical capacity of Li_xTiO_2 for x=1 (µAh/cm^2)	Thickness TiO_2 estimated from growth rate[a] (nm)	Conformal thickness estimated from top-down SEM[b] (nm)	Area enhancement[c]
300	133	19	15	13	9
400	213	30	20	20	11
500	238	34	25	25	10

[a] For a growth rate of 0.05 nm/cycle
[b] For CNS of ~10 nm in thickness and TiO_2 coated on both sides of CNS
[c] Ratio of equivalent/conformal thickness

The equivalent thickness, is the thickness for a dense planar TiO_2 film (~4.2 g/cm^3) equivalent with the total amount of measured Ti by XRF on the sheets. Using this value we also calculated the theoretical capacity of an equivalent films with these thicknesses, also summarised in table 1. The ratio of equivalent thickness and actual conformal thickness gives us the area enhancement of the CNS structures, which is ~10 in all cases. The consistency in conformal thickness and area enhancement points towards good conformal coating of the TiO_2 on the CNS, even though we cannot exclude pinholes and weak spots as a result of the initial nucleation and growth especially deep down in the pores or at folded sheets.

The XRD measurements did not show any TiO_2 signal, which points to the amorphous nature of the TiO_2. This can be explained by the relatively low deposition temperature of 100˚C. Although the use of amorphous TiO_2 is less known in literature compared to anatase, we found that it shows excellent lithium storage properties, which will be elaborated on in the next section. From here on, the 300, 400 and 500 cycle TiO_2 on CNS will be named 15 nm TiO_2-CNS, 20 nm TiO_2-CNS and 25 nm TiO_2-CNS.

3.2. Electrochemical activity of TiO_2/CNS

Cyclic voltammetry at various scan rates was employed to study the kinetic properties of 15, 20 and 25 nm TiO_2-CNS. Figure 3a shows the third cyclic voltammograms (CV) at a scan rate of 0.5 mV/s in the voltage window 3.00 – 0.01 V for bare CNS on TiN and the different TiO_2-CNS samples. A sharp reduction peak can be seen for the bare CNS around 0.1 V and a slightly broader oxidation peak around 0.2 V –in accordance with earlier reports on CNS [6]. In figure 3a, it can also be seen that for all three types of TiO_2-CNS, a broad reduction and oxidation peak around 1.5 V is measured, related to the insertion and extraction of Li^+ in TiO_2, respectively. Broad peaks in the CV is an indication of homogeneous filling of TiO_2 with absence of an immiscible two-phase region; the same response has recently been measured with amorphous TiO_2 nanotubes [18] and porous nanostructured amorphous TiO_2 films [19]. Furthermore, for 15 and 20 nm TiO_2-CNS an additional oxidation peak is measured around 0.7 V; this is likely due to the signal from the CNS which, in the case of the oxidation peak, is shifted to more positive potentials. This oxidation peak seems to only be available for TiO_2 samples with a thin enough coverage of TiO_2, suggesting that a thicker layer will block the lithiation/de-lithiation of the underlying CNS.

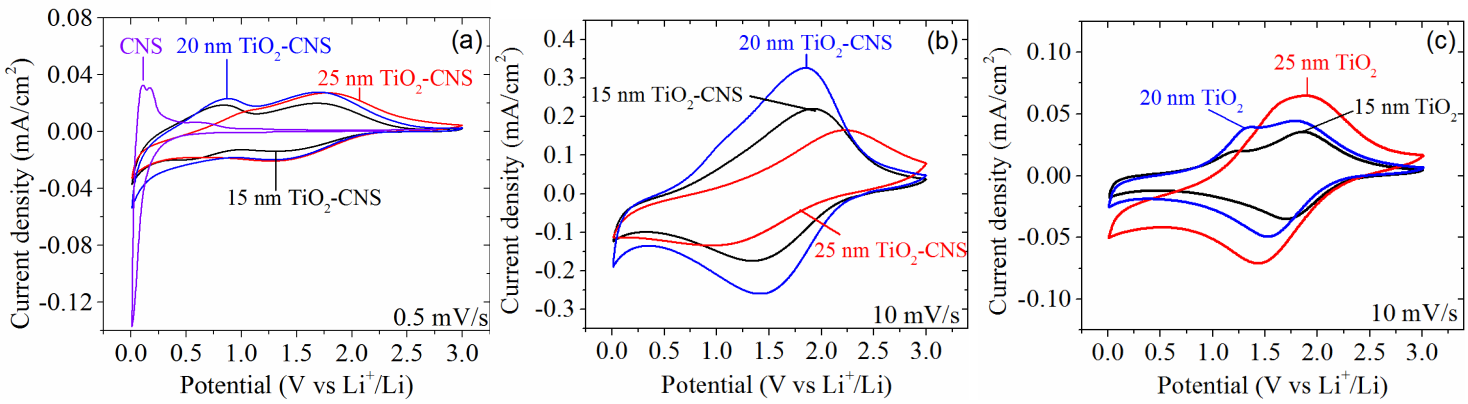

Figure 3. The third cyclic voltammograms of (a) bare CNS, 15, 20 and 25 nm TiO_2-CNS at 0.5 mV/s (b) of 15, 20 and 25 nm TiO_2-CNS at 10 mV/s and (c) of planar 15, 20 and 25 nm TiO_2 on TiN at 10 mV/s.

At a higher scan rate of 10 mV/s (figure 3b), several changes in the response of the different TiO_2-CNS samples is seen. The peak current density of 20 nm TiO_2-CNS is higher compared to that for 15 and 25 nm TiO_2-CNS. Also, the peak potential difference is lowest for 20 nm TiO_2-CNS and largest for 25 nm TiO_2-CNS; indication of an increased overpotential needed for insertion/extraction. Additionally, a small shoulder can still be seen below 1.0 V which can be attributed to the underlying CNS, but with an increased overpotential for de-lithiation. As a reference, TiO_2 was deposited on TiN with a thickness of 15, 20 and 25 nm and a CV was recorded at 10 mV/s (see figure 3c). This also showed the broad characteristic oxidation/reduction peaks for TiO_2 around 1.5 V, with an additional shoulder at 1.2 V which has yet not been identified. However, ongoing tests suggest this shoulder to be related to amorphous TiO_2.

The CNS template provides a large surface area for the ultra-thin TiO_2 electrode. Increasing the thickness of TiO_2 can impede the accessibility of the electrolyte into the TiO_2/CNS pores. This in turns affects the diffusion mechanism and in turn the charge stored. The apparent diffusion mechanisms can be examined by analysing peak currents vs scan rates of recorded CVs. Figure 4a shows the cathodic peak current associated with lithium extraction from TiO_2 as a function of scan rate (0.5 – 500 mV/s) determined from CVs measured for different TiO_2-CNS samples. A similar result is obtained for the anodic peak current. The current measured obeys a power law relation with sweep rate according to [28],

$$i = av^b \quad (2)$$

where *a* and *b* are adjustable parameters. The slope of log i vs log v plot gives the *b* value. A value of *b* close to 0.5 is an indication of a semi-infinite diffusion controlled reaction, while *b* close to unity indicates a surface controlled reaction [20]. Here the *b* value obtained for 15, 20 and 25 nm TiO_2-CNS electrodes are 0.74, 0.75 and 0.56 respectively. The 15 and 20 nm TiO_2-CNS exhibits a mixed surface and semi-infinite diffusion controlled response, whereas the current response for the thicker layer of TiO_2 on the CNS shows semi-infinite length diffusion behaviour.

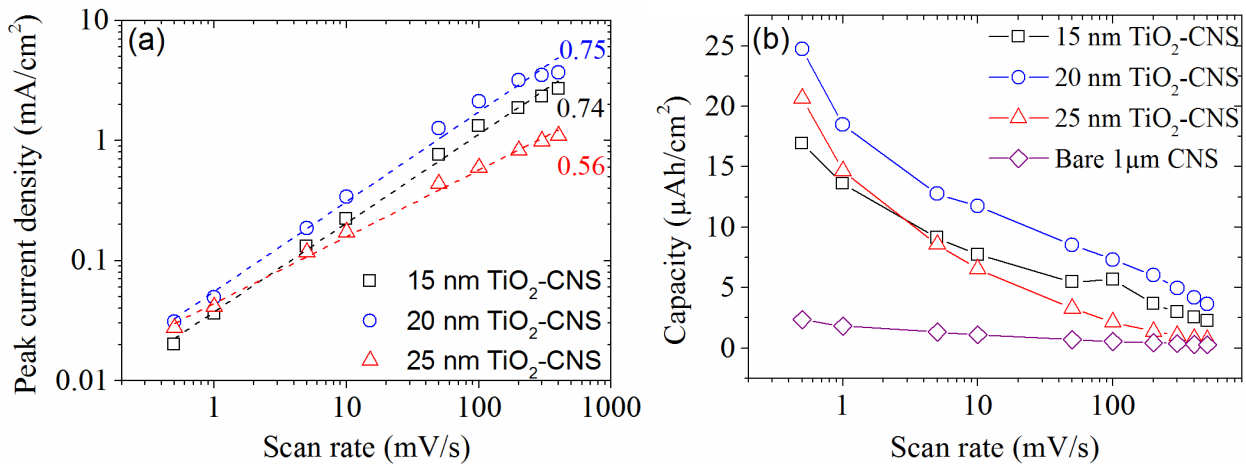

Figure 4. (a) Peak current densities of lithium extraction from different TiO_2 thicknesses on CNS as a function of scan rate. The dotted line shows the slope with the corresponding *b* value. (b) The extracted capacity of de-lithiation (discharging) for the different TiO_2 thicknesses on CNS and bare CNS.

The reason as for why 20 nm TiO_2-CNS shows an optimum in terms of capacity and rate performance can be explained by the optimal balance between the available amount of active material (in this case TiO_2), the accessibility of the liquid electrolyte inside the pores of the whole nanostructure and the availability of the underlying CNS which can also be active. Figure 5 shows a schematic illustrating the different situations when increasing the TiO_2 thickness. More active material becomes available with increased film thickness. Below a certain thickness (≤ 20 nm), the nanostructure allows for good penetration of the electrolyte and in turn short diffusion distances for Li^+ transport (≤ 20 nm). In this case, increasing the TiO_2 thickness will lead to more capacity, as can be seen in the increase in capacity from 15 to 20 nm TiO_2-CNS in figure 4b. However, when a certain TiO_2 thickness is reached (> 20 nm) the pores are becoming clogged, allowing only for the top of the TiO_2-CNS to be in contact with the electrolyte. The lack of electrolyte penetration significantly diminishes the rate at which the

structure can be charged, since Li^+ has to be transported from the electrolyte-TiO_2 interface all the way through the solid TiO_2-CNS (≈0.6 µm) structure.

As a reference, bare CNS were also measured and the capacity as a function of scan rate was also plotted figure 4b. This clearly shows the importance of using TiO_2 combined with CNS; at 0.5 mV/s the capacity of 1 µm tall bare CNS is 2.4 µAh/cm^2 which is an order of magnitude less capacity than 20 nm TiO_2-CNS. This can be explained by the highly porous (~70% free space [4]) structure of the CNS which has very little active material for a given geometric surface area –often ignored when normalizing by weight as is typically done in literature [5], [6], [15].

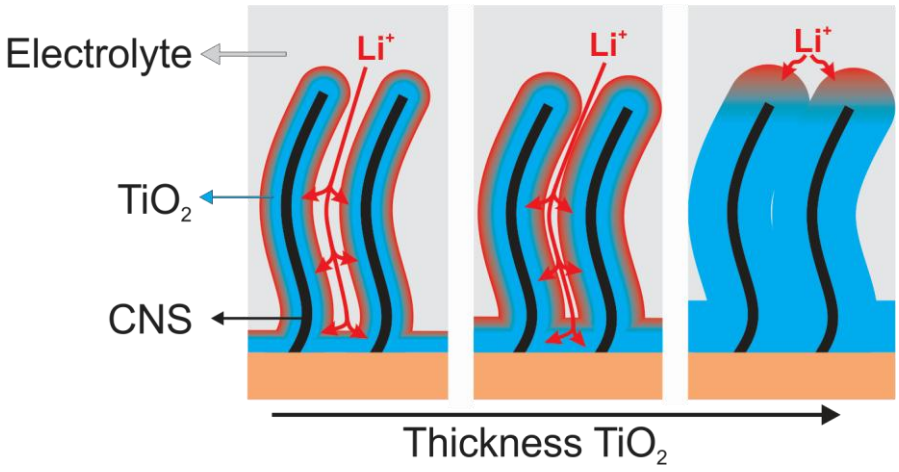

Figure 5. Schematic of lithium insertion into TiO_2-CNS showing the influence of increased TiO_2 thickness. When the TiO_2 thickness is below a certain threshold, the TiO_2-CNS electrode allows for penetration of the electrolyte and offers short diffusion length for Li^+ transport in TiO_2. However, above this threshold the pores are closed off and the electrolyte cannot penetrate the composite electrode, thereby significantly increasing the Li^+ diffusion length which leads to a lower capacity and rate-performance.

3.3. Galvanostatic charge/discharge characteristics of CNS and TiO_2/CNS

The effect of the of the TiO_2 coating thickness on the capacity was also determined by performing galvanostatic charge/discharge experiments. The C-rate was experimentally determined based on the de-lithiation charge measured during the CV at 0.5 mV/s (see figure 4b), which was calculated for 1C to be 17.5, 24.5 and 19.6 µA/cm^2 for 15, 20 and 25 nm TiO_2-CNS respectively. Figure 6a shows the discharge curves obtained from TiO_2-CNS between the voltage ranges 3-0.01 V at a rate of 0.1C. Distinctive voltage regions below and above 1 V are seen for 15 and 20 nm TiO_2-CNS, whereas the whole discharge capacity of 25 nm TiO_2–CNS is mainly achieved above 1 V. The discharge capacities obtained at 0.1C (discharging in 10 h) for 15, 20 and 25 nm TiO_2-CNS are 26

$\mu Ah/cm^2$, 38 $\mu Ah/cm^2$ and 17 $\mu Ah/cm^2$, which is 137%, 127% and 50%, of the theoretical TiO_2 capacity of a film with equivalent thicknesses given in table 1, respectively. Note that we have taken the full theoretical capacity of 1 Li^+ per TiO_2 unit formula, instead of ~0.6 Li^+ which is usually done in literature. The capacities obtained are above the theoretical ones and are attributed to the insertion of Li^+ into the underlying CNS, which also participates at voltages below 1.0 V. As mentioned above, the C-rate was experimentally determined; however this rate can be compared to the theoretical current density based on the complete lithiation/de-lithiation of the total amount of TiO_2 present (see table 1). To charge the different TiO_2-CNS samples in 1h using the theoretical capacities from table 1, we would need to apply 19, 30 and 34 $\mu A/cm^2$ for 15, 20 and 25 nm TiO_2-CNS respectively. The actual current density applied is 93%, 82% and 58% of this theoretical one. It indicates that the current density applied for 15 and 20 nm TiO_2-CNS, is close to the theoretical one, except for 25 nm TiO_2 where a slightly lower current density compared to the theoretical one, was applied. This suggests more time was available for lithium transport in this sample compared to the 15 and 20 nm TiO_2-CNS ones. Taking this into account, 25 nm TiO_2-CNS has clearly the lowest measured capacity and rate performance and utilization of TiO_2 content.

Cycling of the TiO_2-CNS anodes was evaluated up to 30 charge/discharge cycles and is given in figure 6b. All the TiO_2-CNS samples show excellent capacity retention with minimum capacity loss. The 20 nm TiO_2 –CNS retained a discharge capacity of 27.6 $\mu Ah/cm^2$ in the 30^{th} cycle which is about of 98% of the initial value. For 15 and 25 nm TiO_2-CNS, the capacity retention is slightly less than for the 20 nm TiO_2-CNS, which show retention of about ~90% of the initial value after 30 cycles in both cases. SEM images taken (see figure S2) of 15 nm TiO_2-CNS after cycling, showed no noticeable change to the TiO_2-CNS structure. In some regions, deposits on top of the whole TiO_2-CNS structure were seen, which could either be the formation of an SEI, or salt deposits formed during drying of residual electrolyte after disassembly of the cell. Longer term cycling (>30 cycles) experiments would be needed to determine possible failure mechanisms, since no sudden drop in capacity was observed in our case.

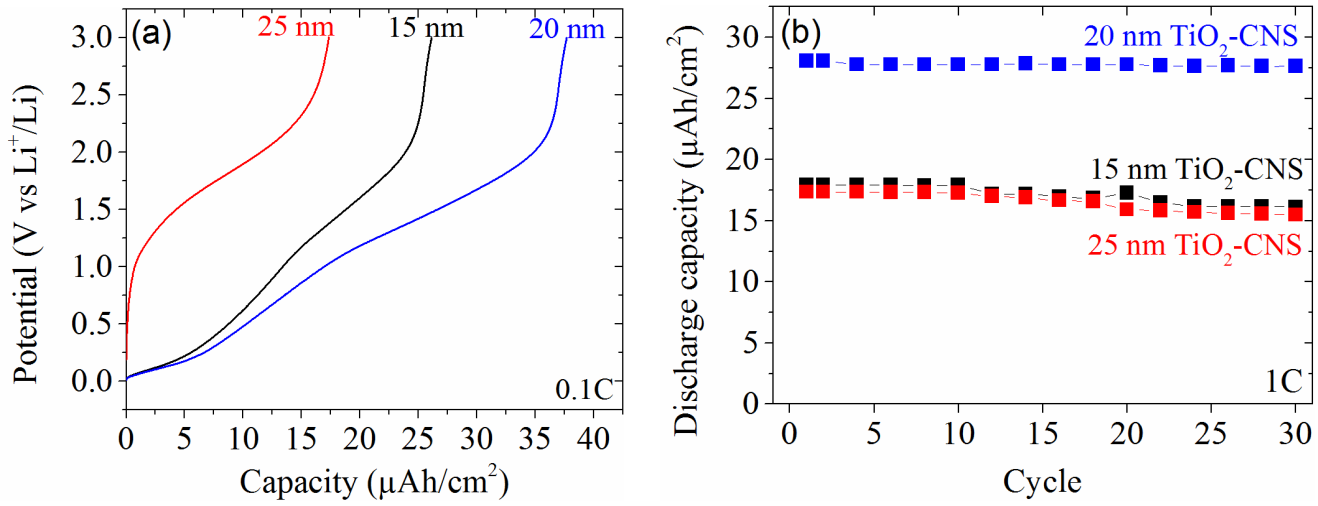

Figure 6.(a) Galvanostatic discharge at 0.1C and (b) a cycling test at 1C for 30 cycles of 15, 20 a 25 nm TiO_2-CNS. The applied current at 1C for the different samples was 17.5, 19.6 and 24.5 μA/cm^2 for 15, 20 and 25 nm TiO_2 respectively.

3.4 Rate capabilities

In order to demonstrate the high-rate capability of the TiO_2/CNS anode, galvanostatic charge/discharge tests were performed at various charging rates. Figure 7a shows the discharge capacity of the three different TiO_2-CNS samples, with varying current rates ranging from 0.1C to 100C. The discharge capacity of 15 and 25 nm TiO_2-CNS at 100C is ~50% and ~4% of the 0.1C capacity, respectively, and 20 nm TiO_2-CNS retains 47% of the original capacity at 5C. It is clear that 20 nm TiO_2-CNS possesses the highest capacity at very high C-rates among the three different TiO_2-CNS, highlighting the excellent rate capabilities of this TiO_2/carbon nanosheet hybrid. In order to discern the capacity associated between the TiO_2 and the CNS, the capacity as a function of C-rate was plotted for two voltage ranges in figure 7b; from 0.01 V to 1.0 V, and 1.0 V to 3.0V. For all three TiO_2-CNS samples, as the charging rate is increased, a smaller amount of capacity is associated with the voltage region below 1.0 V, suggesting that the extraction of Li from the CNS is not possible at higher current rates. The 20 nm TiO_2-CNS seems to have overall more capacity associated to the low voltage region, and retains a larger amount of capacity as a function of C-rate for the high voltage region.

There was good reproducibility of these results showing consistently 20 nm TiO_2-CNS to be superior. This can also be confirmed by comparing the capacities measured with different samples of the same thickness. For example, the capacities at 1C in figure 6b are 17, ~28, 16 μAh/cm^2, for 15, 20 and 25 nm TiO_2-CNS respectively. The capacities

shown in figure 7a at a rate of 1C gave very similar results and allow for a direct comparison, since it concerns different samples of the same TiO_2 thickness.

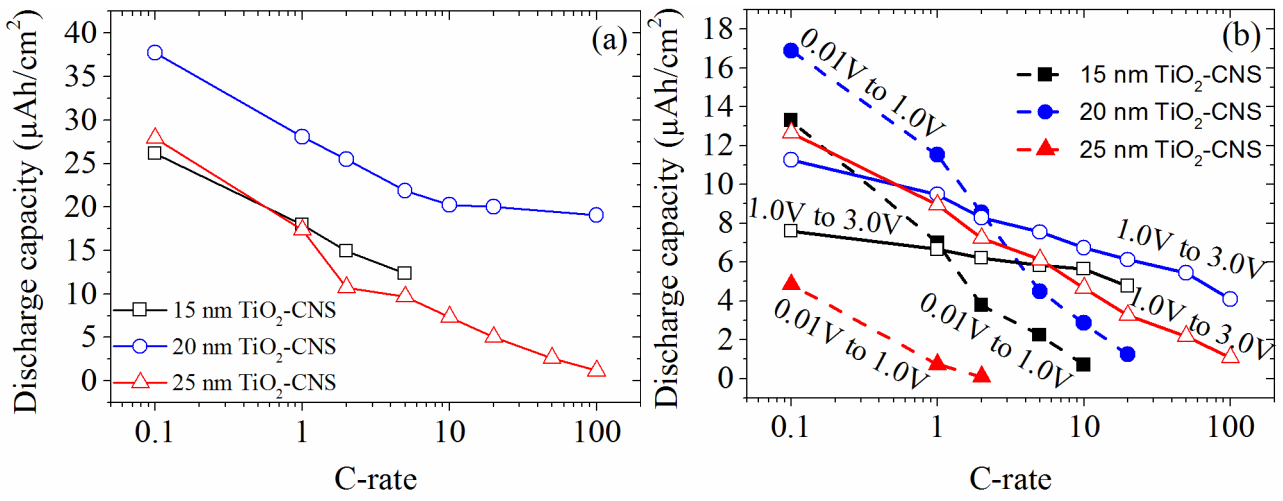

Figure 7. Rate performance of the different TiO_2-CNS samples showing the de-lithiation (discharge) capacity as a function of C-rate. (b) The discharge capacity was taken in two different voltage ranges for the different TiO_2-CNS samples; from 0.01 V to 1.0 V, and 1.0 V to 3.0 V.

4. Conclusions

We have prepared nanostructured amorphous TiO_2 composite electrodes with 300, 400 and 500-cycle ALD on CNS templates, and evaluated the electrochemical performance as the anode layer of LIB. The ALD deposition leads to an area enhancement of a factor ~10 in all cases, with a nominal coverage of 15, 20 and 25 nm on the petal-like corrugated CNS structure. The CNS template functions as an electronic conductive layer and lithium insertion host in addition to giving mechanical support and increased surface area for TiO_2. Cyclic voltammetry showed fast kinetics for 15 and 20 nm TiO_2-CNS in contrast to 25 nm TiO_2-CNS and the highest capacity was found for 20 nm TiO_2-CNS. This was also confirmed with galvanostatic charge-discharge experiments at 0.1C showing capacities of 26, 38 and 17 µAh/cm^2 for 15, 20 and 25 nm TiO_2-CNS, respectively. The rate performance was probed up to 100C (charging in 36 s), where 20 nm TiO_2-CNS showed the best performance with a capacity of 19 µAh/cm^2, retaining 47% of its original capacity. The cycleability of the electrodes were tested by cycling at 1C and showed a capacity retention after 30 cycles of ~98% for 20 nm TiO_2-CNS compared to ~90% for 15 and 25 nm TiO_2-CNS.

The results highlight the importance of depositing a TiO_2 film with a thickness tailored to the CNS substrate, as too thin a TiO_2 film will not effectively use the open space in between CNS, lowering the overall capacity, and too thick a film will block adequate penetration of the electrolyte inside the pores hampering kinetics and in turn the capacity. The optimal film thickness is found with a 20 nm TiO_2-CNS TiO_2/carbon nanosheet hybrid, offering the best in terms of capacity, rate-performance and cycleability. These results show the potential of TiO_2-CNS as a robust and high rate performing electrode. Finally, the IC compatible fabrication steps make possible the integration of TiO_2-CNS electrode material for other micro-power application.

Acknowledgements

The authors wish to thank IWT-Vlaanderen for financial support through the SBO-SOSLION and LAMINALION projects. CD acknowledges the European Research Council for funding (FP7/2007-2013, ERC grant agreement n°239865), and UGent-BOF for funding through GOA-01G01513.

References

[1] M. Wagemaker and F. M. Mulder, "Properties and promises of nanosized insertion materials for Li-ion batteries.," *Acc. Chem. Res.*, vol. 46, no. 5, pp. 1206–15, May 2013.

[2] E. Yoo, J. Kim, E. Hosono, H. Zhou, T. Kudo, and I. Honma, "Large reversible Li storage of graphene nanosheet families for use in rechargeable lithium ion batteries.," *Nano Lett.*, vol. 8, no. 8, pp. 2277–82, Aug. 2008.

[3] G. Wang, X. Shen, J. Yao, and J. Park, "Graphene nanosheets for enhanced lithium storage in lithium ion batteries," *Carbon N. Y.*, vol. 47, no. 8, pp. 2049–2053, Jul. 2009.

[4] D. J. Cott, M. Verheijen, O. Richard, I. Radu, S. De Gendt, S. Van Elshocht, and P. M. Vereecken, "Synthesis of large area carbon nanosheets for energy storage applications," *Carbon N. Y.*, vol. 58, pp. 59–65, Jul. 2013.

[5] H. Kim, Z. Wen, K. Yu, O. Mao, and J. Chen, "Straightforward fabrication of a highly branched graphene nanosheet array for a Li-ion battery anode," *J. Mater. Chem.*, vol. 22, no. 31, p. 15514, 2012.

[6] X. Xiao, P. Liu, J. S. Wang, M. W. Verbrugge, and M. P. Balogh, "Vertically aligned graphene electrode for lithium ion battery with high rate capability," *Electrochem. commun.*, vol. 13, no. 2, pp. 209–212, Feb. 2011.

[7] C. E. Housecroft and A. G. Sharpe, *Inorganic Chemistry*. Prentice Hall Higher Education, 2008.

[8] M. J. Lindsay, M. G. Blackford, D. J. Attard, V. Luca, M. Skyllas-Kazacos, and C. S. Griffith, "Anodic titania films as anode materials for lithium ion batteries," *Electrochim. Acta*, vol. 52, no. 23, pp. 6401–6411, Jul. 2007.

[9] J. Maier, *Physical Chemistry of Ionic Materials: Ions and Electrons in Solids*. John Wiley & Sons, 2004.

[10] Z. Fu and Q. Qin, "Lithium Ion Diffusion Behavior in Laser-Deposited TiO 2 Films," pp. 5505–5510, 2000.

[11] A. Akturk and N. Goldsman, "Electron transport and full-band electron-phonon interactions in graphene," *J. Appl. Phys.*, vol. 103, no. 5, p. 053702, 2008.

[12] H. Cao, B. Li, J. Zhang, F. Lian, X. Kong, and M. Qu, "Synthesis and superior anode performance of TiO2@reduced graphene oxide nanocomposites for lithium ion batteries," *J. Mater. Chem.*, vol. 22, no. 19, p. 9759, 2012.

[13] H.-C. Tao, L.-Z. Fan, X. Yan, and X. Qu, "In situ synthesis of TiO2–graphene nanosheets composites as anode materials for high-power lithium ion batteries," *Electrochim. Acta*, vol. 69, pp. 328–333, May 2012.

[14] D. Wang, D. Choi, J. Li, Z. Yang, Z. Nie, R. Kou, D. Hu, C. Wang, L. V Saraf, J. Zhang, I. A. Aksay, and J. Liu, "Self-assembled TiO2-graphene hybrid nanostructures for enhanced Li-ion insertion.," *ACS Nano*, vol. 3, no. 4, pp. 907–14, Apr. 2009.

[15] C. Ban, M. Xie, X. Sun, J. J. Travis, G. Wang, H. Sun, A. C. Dillon, J. Lian, and S. M. George, "Atomic layer deposition of amorphous TiO2 on graphene as an anode for Li-ion batteries.," *Nanotechnology*, vol. 24, no. 42, p. 424002, Oct. 2013.

[16] M. Rooth, R. a. Quinlan, E. Widenkvist, J. Lu, H. Grennberg, B. C. Holloway, A. Hårsta, and U. Jansson, "Atomic layer deposition of titanium dioxide nanostructures using carbon nanosheets as a template," *J. Cryst. Growth*, vol. 311, no. 2, pp. 373–377, Jan. 2009.

[17] F. Tuinstra, "Raman Spectrum of Graphite," *J. Chem. Phys.*, vol. 53, no. 3, p. 1126, 1970.

[18] W.-H. Ryu, D.-H. Nam, Y.-S. Ko, R.-H. Kim, and H.-S. Kwon, "Electrochemical performance of a smooth and highly ordered TiO2 nanotube electrode for Li-ion batteries," *Electrochim. Acta*, vol. 61, pp. 19–24, Feb. 2012.

[19] Y. Lin, P. R. Abel, D. W. Flaherty, J. Wu, K. J. Stevenson, A. Heller, and C. B. Mullins, "Morphology Dependence of the Lithium Storage Capability and Rate Performance of Amorphous TiO 2 Electrodes," *J. Phys. Chem. C*, vol. 115, no. 5, pp. 2585–2591, Feb. 2011.

[20] J.-Y. Pyun, S.-I., Shin, H.-C., Lee, J.-W., Go, *Electrochemistry of Insertion Materials for Hydrogen and Lithium*. Springer Berlin Heidelberg, 2012, p. 249.

Supplementary information

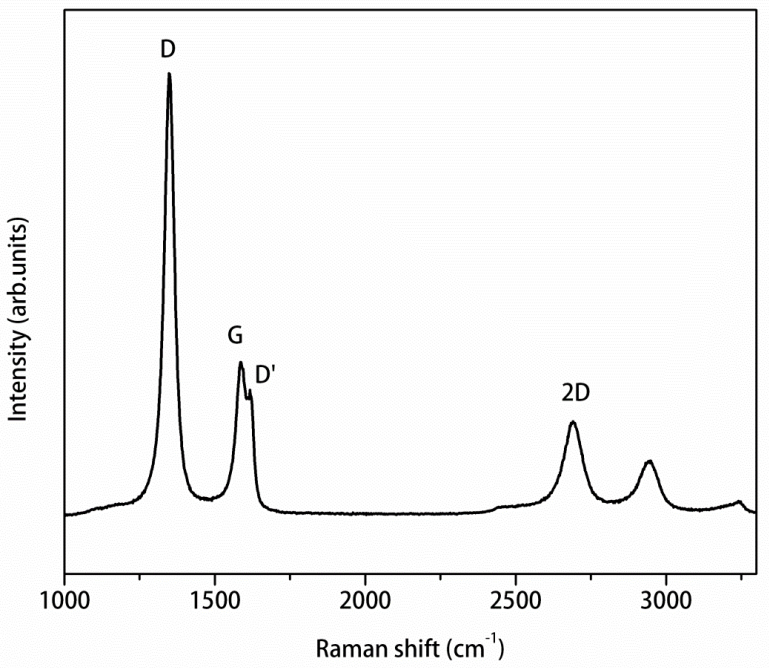

Figure S1. Raman spectroscopy of as received carbon nanosheets on TiN, showing distinguished D and G peaks together with second-order peaks.

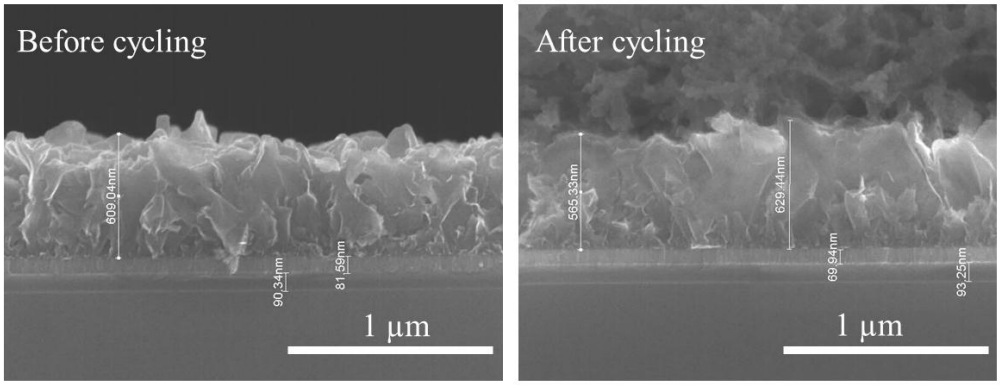

Figure S2. SEM images of 15 nm TiO_2-CNS before and after 30 cycles. The TiO_2-CNS structure did not show any noticeable changes after cycling. In some spots, thick deposits on top of the TiO_2-CNS structure were seen which could be attributed to a SEI formation or otherwise salt deposits arising from drying of residual electrolyte after disassembly of the cell.